# UNDERSTANDING THE SCALAR MESON $q\bar{q}$ NONET

# NILS A. TÖRNQVIST

University of Helsinki, Research Institute for High Energy Physics PB 9, Siltavuorenpenger 20, Fin-00014 Helsinki, Finland

### ABSTRACT

It is shown that one can fit the available data on the  $a_0(980)$ ,  $f_0(980)$ ,  $f_0(1300)$  and  $K_0^*(1430)$  mesons as a distorted  $0^{++}$   $q\bar{q}$  nonet using very few (5-6) parameters and an improved version of the unitarized quark model. This includes all light two-pseudoscalar thresholds, constraints from Adler zeroes, flavour symmetric couplings, unitarity and physically acceptable analyticity. The parameters include a bare  $u\bar{u}$  or  $d\bar{d}$  mass, an over-all coupling constant, a cutoff and a strange quark mass of 100 MeV, which is in accord with expectations from the quark model.

It is found that in particular for the  $a_0(980)$  and  $f_0(980)$  the  $K\bar{K}$  component in the wave function is large, i.e., for a large fraction of the time the  $q\bar{q}$  state is transformed into a virtual  $K\bar{K}$  pair. This  $K\bar{K}$  component, together with a similar component of  $\eta'\pi$  for the  $a_0(980)$ , and  $\eta\eta,\eta\eta'$  and  $\eta'\eta'$  components for the  $f_0(980)$ , causes the substantial shift to a lower mass than what is naively expected from the  $q\bar{q}$  component alone.

Mass, width and mixing parameters, including sheet and pole positions, of the four resonances are given, with a detailed pedagogigal discussion of their meaning.

## 1 Introduction.

As has often been stated in many reviews[1] our present understanding of the light meson mass spectrum is in a deplorable state, especially when one considers the vast amount of data that has been available already for quite some time, and that QCD in principle should solve the hadron spectrum. This is mainly because of the fact that the expectations of most "QCD inspired quark models" fail so dramatically for the scalar mesons, - the Higgs bosons of the hadronic sector.

For the other  $q\bar{q}$  nonets such as the  ${}^3S_1$   $(\rho,\omega,K^*,\phi)$ ,  ${}^3P_2$   $(a_2,f_2,K_2^*,f_2')$ ,  ${}^3P_1$   $(a_1,f_1,K_{1A},f_1')$ ,  ${}^1P_1$   $(b_1,h_1,K_{1B},h_1')$  and even the  ${}^1S_0$   $(\pi,\eta,K,\eta')$  the naive quark model works reasonably well as a rough first approximation. Therefore, few authors doubt that they should be classified as  $q\bar{q}$  states. Certainly, also here there are some "second order effects" such as the observed deviations from ideally mixed states (i.e., mass splittings like  $\rho - \omega$  or  $\Delta - N$  and mixing angles like  $\phi - \omega$  or  $K_{1A} - K_{1B}$ ), for which one has not yet reached consensus as to their full origin. Many authors believe

these deviations are mainly due to gluonic intermediate states, while others[2], including myself, believe the dominant effects come from hadronic loops like  $\phi \to K\bar{K} \to \omega$  etc.

But, for the lightest scalars the  $a_0(980)$ ,  $f_0(980)$ ,  $f_0(1300)$ , and  $K_0^*(1430)$  one has not even reached a clear consensus as to their true nature. Are some of these  $q\bar{q}$ or KK bound states? Or is one of them possibily a glueball? Many authors today believe the  $a_0(980)$  and the  $f_0(980)$  to be KK bound states [1, 3]. This seems, at first, to be a natural assumption, since they lie just a little below the KK threshold. If so, the I=1 and the  $s\bar{s}$  state must be sought for at higher masses. And indeed, there are now candidates for such states: the  $a_0(1450)$  of Crystal barrel[4] (or possibly the questionable  $a_0(1320)$  of GAMS[5]) for the I=1 state, and the LASS  $f_0(1525)$  for the  $s\bar{s}$  state. However, flavour symmetric couplings (which works rather well for the established nonets) would require [6] that their widths should be at least 500 MeV, which is much larger than the observed widths of these candidates. Furthermore, these can have other interpretations (as radial excitations, meson-meson bound states, glueball or threshold effects) like many of the other observed scalars in the much too overpopulated 1370-1720MeV region, where many I=0 candidates[7],  $f_0(1370)$ ,  $f_0(1450)[8]$ ,  $f_0(1525)$ ,  $f_0(1590)$ ,  $f_{0/2}(1710)$ , do not find a place in the  $q\bar{q}$  quark model. One of these could be a glueball, another a deuteronlike state (deuson)[9] etc. In order to reach a better conclusion of their true nature it would of course be very helpful if at least the lightest scalar  $q\bar{q}$  nonet would be resolved.

It is fundamental also in many other respects to have a good model of the scalars, in particular for understanding chiral symmetry breaking, nuclear forces and of course confinement. For chiral symmetry breaking it would be important to know: Where is the sigma meson? Is it the  $f_0(980)$ , or the  $f_0(1300)$ , or must its mass be pushed to infinity? How does the Nambu–Jona-Lasinio mechanism[10] work for the light spectrum? Is the pion both the Nambu-Goldstone boson and the I=1  $^1S_0$   $q\bar{q}$  meson, as most authors believe, or does one have to look for the  $q\bar{q}$  pion at higher masses, as questioned e.g., by Georgi and Manohar[11].

For nuclear forces, and for the understanding of the  $\Delta I = 1/2$  enhancement in  $K \to 2\pi$  and  $K_{l4}$  decay[12], one would like to have a very light  $\sigma$ , in the range of 600-900 MeV, coupling strongly to  $\pi\pi$ ; a meson which does not seem to exist. The lightest scalar is the  $f_0(980)$ , which behaves more like an  $s\bar{s}$  or a  $K\bar{K}$  state coupling weakly to  $\pi\pi$ , while the  $f_0(1300)$  seems too heavy. In this paper I shall suggest a new solution to this old question.

Finally, for confinement the scalars play an important role in building through tadpole diagrams the hadronic bag, within which the quarks reside. They are important for the confinement energy, for the  $q\bar{q}$  condensate, and for the difference between constituent and chiral quark masses. Thus, they are crucial for the understanding of all hadronic masses.

Many authors have recently studied some of the scalars we discuss here, but generally these have tried to fit at the same time only one or two of them and not the whole flavour nonet simultaneously. Bugg et al.[13] and Morgan and Pennington[14] have

made detailed fits with many parameters to  $\pi\pi$  amplitudes using general techniques of unitarity, analyticity and the K-matrix. Janssen et al.[15] studied the  $a_0(980)$  and  $f_0(980)$  in a meson exchange model for  $\pi\pi$  and  $\pi\eta$  interactions, Achasov[16] studied the low energy  $\pi\pi$  data also with meson exchange and Adler zero constraints. Kaminsky et al. [17] studied the  $a_0(980)$  and  $f_0(980)$  using a coupled channel model concluding that the  $f_0(980)$  is a " $K\bar{K}$  molecule". Earlier many authors[18] have discussed unitarity and analyticity for the hadron spectrum.

The results presented here is a very much improved calculation and discussion of a short letter[19] 14 years ago. In particular, I have included constraints from Adler zeroes, which considerably improve the agreement with data close to thresholds without increasing the number of parameters.

In the following I first discuss the general ingredients and properties of the unitarized quark model (UQM) in Sec.2. Although this section does contain new results and new material to resonance phenomena and the UQM, it can perhaps be skimmed by those who just want to understand the fits. It is written in a rather pedagogical way and emphasizes some facts, which are often forgotten by many model builders. Sec.3 is the central chapter of this paper, where the actual application and fits to the scalar nonet are presented while in the concluding remarks, Sec.4, some comments on these results are discussed.

## 2. The unitarized quark model.

The UQM incorporates unitarity and physically acceptable analyticity with resonances in a way, by which one maintains a simple and transparent physical interpretation of the introduced resonance parameters. It is a kind of advanced form of the classical work of Weisskopf and Wigner[20]. The UQM was applied to many different hadrons[21], and it can explain the signs[6] and magnitudes of deviations from ideal mixing, and many mass splittings. Particularly significant is the large splitting between  $\Upsilon(5S)$  and  $\Upsilon(4S)$ , which cannot be understood in single channel potential models (where the predicted splitting is over 50 MeV too small) nor by gluonic exchange. At present there is no other mechanism than hadronic shifts from the loops  $\Upsilon(nS) \to D\bar{D}$ ,  $D\bar{D}^*$  etc.  $\to \Upsilon(mS)[22]$ , which can account for this large splitting.

### 2.1 General formulation

In the UQM one writes for the partial wave amplitudes (PWA) in "Argand units" a factorized matrix form:

$$A_{ij}(s) = T_{ij}(s)(k_i k_j)^{\frac{1}{2}} = \sum_{\alpha\beta} G^{\dagger}(s)_{i\alpha} P_{\alpha\beta}(s) G_{\beta j}(s) , \qquad (1)$$

where one sums over the resonance indices  $\alpha$  and  $\beta$  (for e.g.,  $f_0(980)$ ,  $f_0(1300)$  etc.) and where i and j denote the two-body thresholds (e.g.,  $\pi\pi$ ,  $K\bar{K}$  etc.). The matrices  $G_{\alpha i}(s)$  include coupling constants  $(g_{\alpha i})$ , phase space (and angular momentum) factors, and form factors. We write for real s:

$$G_{\alpha i}^{2}(s) = g_{\alpha i}^{2} \frac{k_{i}(s)}{\sqrt{s}} F_{\alpha i}^{2}(s) \theta(s - s_{th,i}) , \quad s_{th,i} = (m_{A_{i}} + m_{B_{i}})^{2} , \qquad (2)$$

where  $k_i(s) = [\lambda(s, m_{A_i}^2, m_{B_i}^2)/s]^{1/2}/2$  is the cm momentum of the two intermediate particles  $A_i$  and  $B_i$ . The form factors  $F_{\alpha i}(s)$  are at this stage still quite arbitrary, except for the fact that we shall require them to vanish sufficiently fast at  $\infty$  (In the following we generally suppress the index  $\alpha$  on the  $F_{\alpha i}$ , since in our application in this paper we assume this does not depend on the resonance). One expects them to be smooth functions of s, which include angular momentum barriers, radial nodes, and in principle the left hand cuts. In the quark pair creation model[23] they are given by an overlap of the three hadronic wave functions multiplied by a matrix element for the  $q\bar{q}$  pair creation. In fact, the  $F_i(s)$  include most of the model dependence of our scheme.

For  $q\bar{q}$  resonances the propagator matrix  $P_{\alpha\beta}(s)$  depends on the bare mass parameters  $m_{0,\alpha}$ , and on the mass shifts  $Re\Pi_{\alpha\beta}(s)$ , and the width-like functions  $Im\Pi_{\alpha\beta}(s)$ , which together determine the analytic vacuum polarization functions  $\Pi_{\alpha\beta}(s)$ .

$$P_{\alpha\beta}^{-1}(s) = (m_{0,\alpha}^2 - s)\delta_{\alpha\beta} + \Pi_{\alpha\beta}(s) , \qquad (3)$$

The unitarity condition,  $(A - A^{\dagger})/(2i) = AA^{\dagger}$ , takes a very simple form determining the imaginary part of  $\Pi_{\alpha\beta}(s)$ :

$$Im\Pi_{\alpha\beta}(s) = -\sum_{i} G_{\alpha i}(s)G_{i\beta}^{\dagger}(s) = -\sum_{i} g_{\alpha i}g_{\beta i}\frac{k_{i}(s)}{\sqrt{s}}F_{i}^{2}(s)\theta(s - s_{th,i}) . \tag{4}$$

Since the functions  $\Pi_{\alpha\beta}(s)$  are analytic functions with only right hand cuts, we can write dispersion relations for the real parts  $Re\Pi_{\alpha\beta}(s)$ :

$$Re\Pi_{\alpha\beta}(s) = \frac{1}{\pi} \mathcal{P} \int_{s_{th,1}}^{\infty} \frac{Im\Pi_{\alpha\beta}(s')}{(s'-s)} ds' . \tag{5}$$

These need no subtractions, since we require that the hadronic form factors  $F_i(s)$  make  $Im\Pi_{\alpha\beta}(s)$  go to zero sufficiently fast at infinity because hadrons have finite size. Thus the integrals are finite and we need not add any polynomial to  $Re\Pi_{\alpha\beta}(s)$  apart from the  $m_{0,\alpha}^2 - s$  term, which we already included in  $P^{-1}$  in order to have the  $q\bar{q}$  resonances as CDD[24] poles. By defining  $Re\Pi_{\alpha\beta}(s)$  through the dispersion relation one automatically satisfies physically correct analytic properties, i.e., one gets no spurious poles nor cuts and right asymptotic behaviour. (See discussion in Sec. 2.7. below). Thus, once we have a model for the  $G_{\alpha i}(s)$  and the bare masses, the PWA can be calculated.

By having the functions  $\Pi_{\alpha\beta}(s)$  in the inverse propagator one automatically sums over all iterated loop diagrams of the Born terms (see the diagrams in Fig. 1a,b), such that the amplitude includes an infinite set of diagrams of the form shown in Fig. 1c. In Fig. 1 we have included, in addition to the  $q\bar{q}$  resonance terms also contact terms (Fig. 1b) to be discussed in subsection 2.5.

Fig. 1. The Born term for (a) the bare  $q\bar{q}$  resonances, for (b) the contact terms, and (c) the loops summed by the functions  $\Pi_{\alpha\beta}(s)$  in the inverse propagator.

## 2.2 A single resonance

Some special cases are instructive. For a single resonance P(s) is one-dimensional, and assuming real  $G_i(s)$  (as can quite generally be done for  $2 \to 2$  particle amplitudes) the PWA takes the form:

$$A_{ij} = \frac{G_i(s)G_j(s)}{m_0^2 + Re\Pi(s) - s - i\sum_i G_i^2(s)} = \frac{m_{BW}(\Gamma_i(s)\Gamma_j(s))^{\frac{1}{2}}}{m^2(s) - s - im_{BW}\Gamma_{tot}(s)}.$$
 (6)

One recovers a generalization of the familiar Breit-Wigner form in the second expression of eq.(6), where one has put  $\Gamma_i(s) = G_i^2(s)/m_{BW}$ . Here  $m^2(s) = m_0^2 + Re\Pi(s)$  is the "running squared mass", which is given by the bare squared mass plus the generally negative mass shift  $Re\Pi(s)$ . This function is approximately constant only in special situations, e.g., if one is far from all thresholds. For S-waves the s-dependence is particularly important, since  $Re\Pi(s)$  has square root cusps at each threshold, and near such a threshold there is a dramatic s-dependence. See Fig. 2a,b where we display the running mass and  $Im\Pi(s)$  for the  $K_0^*$  and for the  $a_0$  as obtained in the fit presented in the next section. Note in particular the strong cusp at the  $K\eta'$  threshold. Since the  $K_0^*(1430)$  lies sufficiently below this threshold the s-dependence of  $m^2(s)$  is here not so crucial as it is for the  $a_0(980)$  and for the  $f_0(980)$  resonances, which lie essentially right at the  $K\bar{K}$  threshold. One sees from Fig. 2b that for the  $a_0(980)$  all

Fig. 2. (a) The real and the imaginary parts of the function  $m^2(s) = m_{0i}^2 + \Pi(s)$  for the  $K_0^*(1430)$  resonance plotted as a function of  $\sqrt{s}$ . Note the strong cusp at the  $K\eta'$  threshold and that the  $K\eta$  threshold essentially decouples because of the small coupling constant. The dashed curve is s, which crosses the running mass  $\text{Re}[m^2(s)]$  at the BW mass.

(b) As in (a) but for the  $a_0(980)$  resonance. Note that the three thresholds have similar coupling strengths and that they lie much closer together than in (a). Therefore the large mass shift for  $a_0(980)$ . The dashed curve is s, which crosses  $Re[m^2(s)]$  at the BW mass.

three thresholds  $\pi \eta$ ,  $K\bar{K}$ , and  $\pi \eta'$  lie close to each other. They all contribute to a large  $a_0(980)$  mass shift and a strong s-dependence in the running mass.

## 2.3 Two and more resonances

When one considers two resonances the propagator matrix becomes two-dimensional and has important off-diagonal elements given by  $\Pi_{\alpha\beta}(s)$ . In general, one gets an s-dependent complex mixing angle between the two states, since the mass and propagator matrices are diagonalized by a complex orthogonal matrix. This generates e.g., OZI violation although the bare states are assumed ideally mixed  $q\bar{q}$  states.

A special, instructive case is obtained if one has only one threshold, or if the coupling constants of the two resonances are proportional to each other,  $G_{2i}(s) = \alpha(s)G_{1i}(s)$ . Such a proportionality can hold when the resonances have the same flavour content, say two  $K_0^*$ 's with flavour symmetric couplings. Then both bare states have couplings proportional to the same  $SU_{3f}$  Clebsch-Gordan coefficients, which are given by the general trace formulae:

$$g_{\alpha,i} = gTr[\mathcal{M}_{A_i}\mathcal{M}_{B_i}\mathcal{M}_{C_\alpha}]_{C_{A_i}C_{B_i}C_{C_\alpha}}, \qquad (7)$$

where  $A_i$ ,  $B_i$ ,  $C_\alpha$  stand for the three mesons involved at the vertex  $C_\alpha \to A_i + B_i$ , and  $\mathcal{M}_{A_i}$  is the 3x3 flavour matrix for meson  $A_i$ . Either the symmetric or the antisymmetric trace is to be taken, depending on the sign of the product the three charge conjugation quantum numbers. For the  $0^{++} \to 0^{-+}$  vertices, which we discuss in this paper it is thus the symmetric trace. Then after some algebra one can reduce the expression (1) to:

$$A_{ij} = \frac{[1 + \alpha^2(s)]G_{1i}(s)G_{1j}(s)}{(m_{0,1}^2 - s)(m_{0,2}^2 - s)/(\bar{m}^2(s) - s) + \Pi(s)},$$
(8)

where

$$\alpha(s) = G_{2i}(s)/G_{1i}(s) = g_{2i}F_{2i}(s)/[g_{1i}F_{1i}(s)], \qquad (9)$$

$$\bar{m}^2(s) = \frac{m_{0,1}^2 \alpha^2(s) + m_{0,2}^2}{1 + \alpha^2(s)},$$
 (10)

$$Im\Pi(s) = -[1 + \alpha^2(s)] \sum_{i} G_{1i}^2(s) ,$$
 (11)

$$Re\Pi(s) = \frac{1}{\pi} \mathcal{P} \int_{s_{th}}^{\infty} \frac{Im\Pi(s')ds'}{s'-s} . \tag{12}$$

(13)

This shows explicitly how resonances must be "added multiplicatively" because of unitarity. Wheras the single resonance form (6) gives one loop in the Argand diagram

<sup>\*</sup>The result looks almost like magic if one starts from eq. (1), but it is easily found starting with the K or even better with the B matrix defined in Sec. 2.7.

the two resonance form (8) gives two loops with a zero in the amplitude at  $s = \bar{m}^2(s)$ . Note that the zero is unshifted, which could be phrased as a theorem: A zero in the PWA in the physical region remains a zero after unitarization.

I find it rather surprising that this quite simple generalization (8) of the BW formula to the case of two resonances is not found in the literature, although it could be very useful phenomenologically e.g., when studying two resonances in channels with nonzero flavour like  $K\pi$ , where eq. (9) can hold.

A special case of eq.(8) is also instructive, and this bears some resemblance to the "S\* effect", i.e. the  $f_0(980)$  discussed below: Imagine two nearly degenerate resonances both with large couplings to common channels. Unitarity will shift both masses and the phase shift will pass 90° for the first and 270° for the second resonance, close to each other in energy. Thus, one gets a narrow resonance structure in the form of a dip between two broad bumps. How can this this come about? In fact, when looking at the original form, eq.(1), the  $2 \times 2$  mass matrix in the propagator, when diagonalized [cf. next subsection 2.4, eqs.(17-19)] results in a mixing between the two resonances, such that one of them nearly decouples from the thresholds, while the other gets very large couplings (cf. eq.(18) below). Thus in terms of eigenvalues one has one very broad and one very narrow resonance, the latter producing a strong dip in the broad resonance bump. Or in other words, two inherently broad resonances can together produce one very narrow one!

For the  $f_0(980)$  this mechanism is of course not the whole story. Here the couplings are not proportional to each other, i.e., they do not satisfy eq.(9), and the  $K\bar{K}$  threshold plays a crucial role in bringing the two resonances close to each other, but loosely speaking a variant of this mechanism is operative. A somewhat similar phenomenon appears also for the two axial  $K_1$  mesons, which are near 45° mixtures of the  $K_{1A}$  and  $K_{1B}$ , (which belong to the  $1^{++}$  and  $1^{+-}$  nonets) such that one of them nearly decouples from  $K^*\pi$  and the other decouples from  $K\rho$  (cf. Katz and Lipkin[2]). Also in the late sixties there were discussions of similar effects in the connection with split resonances[25] (in particular the now well forgotten "split  $a_2$ ").

For the more general case with two (or more) resonances and many thresholds with different kinds of couplings, like  $(u\bar{u} + d\bar{d})/\sqrt{2}$  and  $s\bar{s}$  states, one does not gain much insight by trying to reduce the matrix form of the propagator of eq. (1) algebraically. The "reduced" formula becomes quite complicated because of the energy dependent complex mixing induced. But, fortunately eq. (1) is as it stands already quite transparent physically, and easy to compute numerically.

# 2.4 Breit-Wigner masses and widths, pole positions and resonance mixings.

For the single resonance case eq.(6) the Breit-Wigner (90°) mass is given by the s-value where  $m_0^2 + Re\Pi(m_s) - s$  vanishes or by

$$m_{BW}^2 = m_0^2 + Re\Pi(m_{BW}^2) ,$$
 (14)

while the widths could be defined as  $\Gamma_i = G_i^2(m_{BW}^2)/m_{BW}$  as in eq.(6). However, if the slope of  $Re\Pi(s)$  at the resonance is large, one should correct for this and absorb the slope into the s term by dividing both numerator and denominator in eq.(6) by the same term, and define the BW widths by

$$\Gamma_i^{BW} = \frac{G_i^2(m_{BW}^2)/m_{BW}}{1 - \frac{d}{ds}Re\Pi(m_{BW}^2)} , \qquad \Gamma_{tot}^{BW} = \sum_i \Gamma_i^{BW} .$$
 (15)

This renormalization of the widths and couplings (which is also familiar in field theory) has a clear physical interpretation: Below each threshold the  $q\bar{q}$  pair produces virtual pairs of the two mesons, and the probability for such pairs is proportional to  $-\frac{d}{ds}\Pi_i(s) = -\frac{1}{\pi}\int ds' Im\Pi(s')/(s-s')^2$ . The  $q\bar{q}$  wave function obtains meson-meson components  $|A_iB_i>$ :

$$|\psi\rangle = [|q\bar{q}\rangle + \sum_{i} [-\frac{d}{ds} Re\Pi_{i}(s)]^{\frac{1}{2}} |A_{i}B_{i}\rangle] / [1 + \sum_{i} (-\frac{d}{ds} Re\Pi_{i}(s)].$$
 (16)

Each  $|A_iB_i>$  component has in configuration space an exponential radial tail, whose slope is inversely proportional to how much below the threshold the state is. Thus for the  $a_0(980)$  and  $f_0(980)$  the size of the  $K\bar{K}$  component grows both in spatial size and in absolute magnitude the closer to the threshold from below the resonance is. The reduction of the width and coupling in eq. (15) is physically due to the fact that only the  $q\bar{q}$  component annihilates directly to  $\pi\eta$  respectively  $\pi\pi$ . The  $|K\bar{K}>$  part is rather inert, since it must first transform into  $q\bar{q}$  near the origin and then into  $\pi\eta$  or  $\pi\pi$ . Above the threshold the situation is very different; the  $K\bar{K}$  component vanishes since it can simply fall apart, and gives an absorptive part to the wave function. The slope of  $Re\Pi(s)$  is here generally positive implying that the BW width is in fact enhanced.

In the case when one has many resonances one can define the generalization of BW masses and widths by first diagonalizing the mass matrix and propagator by a complex orthogonal matrix  $\mathcal{O}(s)$ , which also rotates the couplings which now become complex:

$$m_{diag,\alpha}^2(s) = \sum_{\alpha'\beta'} \mathcal{O}_{\alpha\alpha'}^{-1}(s) [m_{0,\alpha'}^2 \delta_{\alpha'\beta'} + \Pi_{\alpha'\beta'}(s)] \mathcal{O}_{\beta'\beta}(s) , \qquad (17)$$

$$g'_{\alpha i}(s) = \sum_{\beta} \mathcal{O}_{\alpha \beta}^{-1}(s) g_{\beta i} , \qquad (18)$$

$$A_{ij} = \sum_{\alpha} \frac{g'_{\alpha i}(s)g'_{\alpha j}(s)}{m_{diag,\alpha}^2(s) - s} F_i^2(s) \frac{k_i(s)}{\sqrt{s}}. \tag{19}$$

One can then define the BW masses in the multiresonance case as the energies where  $Re[m_{diag,\alpha}^2(s)] - s$  vanishes. This definition has the advantage that this mass in principle is the same in all channels i. We shall here use this definition. Other definitions, such as the energies where the phase of each term in the sum (19) is 90°,

or the energies where their absolute value of each term is maximal, do not have this property. But, the analogy with the single resonance case is not simple, because the coupling constants  $g'_{\alpha i}(s)$  are now complex and energy dependent and furthermore, there is a background from other resonance tails. As an example the mixing angle between the  $s\bar{s}$  and  $(u\bar{u}+d\bar{d})/\sqrt{2}$  components in the  $f_0(980)$  or  $f_0(1300)$  is complex and is strongly s-dependent. It has a different value at the  $f_0(980)$  than at  $f_0(1300)$ , and furtermore it will be different when evaluated at the BW mass, than at the pole position for the same data and model.

The pole positions have the advantage that only here does the process factorize into production and decay independently of the background. These are determined by the complex s value and sheet number, where the the whole inverse propagator  $m_0^2 + \Pi(s) - s$  vanishes, or more generally where  $\det[P^{-1}(s)]$  vanishes. For each threshold the number of sheets is doubled, and the sheet number is determined by the signs of  $Im(k_i)$ . The same resonance can, in general, have several image poles on different sheets, which considerably complicates matters since the same resonance can have more than one nearby pole (See Morgan and Pennington[14] and [26] for a discussion). In our model for the  $f_0(980)$  and  $f_0(1300)$  we have 5 thresholds, which means there are 32 sheets, some of which could even have 2 poles each! To find the nearest poles one must analytically continue  $\Pi_{\alpha\beta}(s)$  defined above at the first sheet only just above the real axis. At the first sheet we can calculate  $\Pi_{\alpha\beta}(s)$  by generalizing eq.(5) to complex s values on the first sheet (I) by the Cauchy integral around the cut on the real x axis:

$$\Pi_{\alpha\beta}^{I}(s) + \frac{1}{\pi} \int_{s_{th}}^{\infty} \frac{Im\Pi_{\alpha\beta}(x)dx}{x - s} . \tag{20}$$

This is discontinuous across the cut. To get to the second sheet (II) one must add a term:

$$\Pi_{\alpha\beta}^{II}(s) = \Pi_{\alpha\beta}^{I}(s) + 2i\bar{G}_{\alpha 1}(s)\bar{G}_{\beta 1}(s) , \qquad (21)$$

where  $\bar{G}_{1\alpha}(s)\bar{G}_{1\beta}(s)$  is given by essentially the same expression as eq. (2) or eq.(4), but now without the theta function, and defined also for complex values of s. Near the real axis  $\Pi_{\alpha\beta}^{II}(s)$  has the opposite sign compared to  $\Pi_{\alpha\beta}^{I}(s)$  in the imaginary part above threshold. Again below threshold, the cusp in the real part changes sign. Explicitly the additional term is given by:

$$i\bar{G}_{\alpha i}(s)\bar{G}_{\beta i}(s) = -g_{\alpha i}g_{\beta i}\sqrt{-\lambda(s, m_{A_i}^2, m_{B_i}^2)}s^{-1}F_i^2(s)$$
, (22)

or with the Adler zero constraints and flavour symmetric couplings (See sec. 2.5):

$$i\bar{G}_{\alpha i}(s)\bar{G}_{\beta i}(s) = -\gamma_{\alpha i}\gamma_{\beta i}(s - s_{A,i})\sqrt{-\lambda(s, m_{A_i}^2, m_{B_i}^2)} \quad s^{-1}F_i^2(s) , \quad \text{where} \quad (23)$$

$$\gamma_{\alpha i} = \gamma[Tr[\mathcal{M}_{A_i}\mathcal{M}_{B_i}\mathcal{M}_{C_\alpha}]_+] \quad . \quad (24)$$

In order to get to the third sheet (III) two terms from the first and second threshold must be added

$$\Pi_{\alpha\beta}^{III}(s) = \Pi_{\alpha\beta}^{I}(s) + 2i\bar{G}_{\alpha 1}(s)\bar{G}_{\beta 1}(s) + 2i\bar{G}_{\alpha 2}(s)\bar{G}_{\beta 2}(s) , \qquad (25)$$

while to get to the fourth sheet one should only add the second term. In general, with the signs of  $Imk_i$  given by the sheet number (n) one should add  $2i\bar{G}_{\alpha j}(s)\bar{G}_{\beta j}(s)$  for each threshold j with negative  $Imk_j$ :

$$\Pi_{\alpha\beta}^{n}(s) = \Pi_{\alpha\beta}^{I}(s) + 2i\sum_{j} \bar{G}_{\alpha j}(s)\bar{G}_{\beta j}(s)\theta(-Imk_{j}). \qquad (26)$$

## 2.5 Background and t and u channel exchange terms.

For the case of a nonresonant background term as given e.g., by a contact term (Fig. 1b) one still has an expression very similar to the one above, but with the  $m^2-s$  terms in the propagator replaced by a constant, which could be chosen = 1. But, in order to have the same dimensions for the coupling constants of the background as for the resonances we put this constant  $=\pm M^2$  (with dimension GeV<sup>2</sup>), and with the sign allowing for constructive or destructive interference. Then for the contact terms we have:

$$P_{\alpha\beta,\text{contact}}^{-1}(s) = \pm M_{\alpha}^2 \delta_{\alpha\beta} + \Pi_{\alpha\beta}(s) . \tag{27}$$

The same constraints from unitarity and analyticity still apply as given by eqs. (2,4,5), i.e.,  $\Pi_{\alpha\beta}(s)$  is given by the same formulas as before although the interpretation of the coupling constants now refers to the background.

We can thus add a background term to each resonance by doubling the dimension for the propagator, such that for the case of one resonance and a background one writes a  $2 \times 2$  inverse propagator matrix

$$P_{\alpha\beta}^{-1}(s) = \begin{pmatrix} m_0^2 - s & 0\\ 0 & \pm M^2 \end{pmatrix} + \Pi_{\alpha\beta}(s) .$$
 (28)

The same formulas for  $\Pi_{\alpha\beta}(s)$  still apply, but since  $\Pi_{\alpha\beta}(s)$  has off diagonal terms the background mixes with the resonance in a complex although specified way just as in the two resonance case. An important special case appears when the background couplings are proportional to the resonance couplings, as is the case when one assumes the same flavour structure for resonance and background  $(g_{\alpha i,backg} = \alpha g_{\alpha i,reson.})$ . In this case when one algebraically reduces the dimension of the propagator matrix one gets the same resonance formula, but with a modified  $G_{\alpha i}(s)$ . With the same original  $F_i(s)$  for resonance and background one needs only to substitute  $g_{\alpha,i}^2 \to g_{\alpha,i}^2[1 \pm \alpha^2(m_{0,\alpha}^2 - s)/M^2]$ . This new linear factor implies that there is a zero in the amplitudes, which we identify with the Adler zeroes near s = 0. Thus by adding the resonance and contact term with a definite relative weight one introduces the Adler

zeroes[27] needed from current algebra. We let the Adler zeroes be at  $s = s_{A,i}$ . All this is accomplished by the simple substitution:

$$g_{\alpha i}^2 F_i^2(s) \rightarrow \gamma_{\alpha i}^2(s - s_{A,i}) F_i^2(s)$$
, or (29)

$$G_{\alpha i}(s)G_{\beta i}(s) \rightarrow \gamma_{\alpha i}\gamma_{\beta i}(s-s_{A,i})F_i^2(s)\frac{k_i(s)}{\sqrt{s}}\theta(s-s_{th,i}),$$
 (30)

where we now have introduced dimensionless coupling constants  $\gamma_{\alpha i}$ , which are related by flavour symmetry eq.(24).

One can of course in a similar way include more complicated dynamics coming from t- and u-channel exchanges. By making a partial wave projection of the Born term one first determines the  $G_{\alpha i}(s)$  and the function, which should replace  $M^2$  or  $m_0^2 - s$  above, which will contain logarithms etc. Then one sums the iterated higher order diagrams by the above unitary formalism.

# 2.6 The UQM when two pseudoscalars are produced by some other reaction.

Much of the physics of  $\pi\pi$  and  $K\pi$  systems can be learnt from other reactions than the two-body reactions discussed above. Such reactions are  $\Upsilon' \to \Upsilon\pi\pi$ ,  $K \to \pi\pi e\nu$  or central production of  $\pi\pi$  in pp collisions. The UQM can easily be modified in order to be applicable also to such processes. All one needs to do (provided the strong interactions in the final state is only between the two pseudoscalars) is to replace the vertex functions  $G_{\beta i}(s)$  at one of the two vertices by some other real functions  $C_{\beta p}(s)$ , parametrized in an appropriate way for the production, while the propagator matrix including the bare masses and the  $\Pi_{\alpha\beta}(s)$  functions, and  $G_{\beta i}(s)$  at the second vertex for the decay remain as above:

$$\mathcal{F}_{ip}(s) = \sum_{\alpha\beta} G^{\dagger}(s)_{i\alpha} P_{\alpha\beta}(s) C_{\beta p}(s) , \qquad (31)$$

This guarantees that the Watson final state theorem, and unitarity in general, is automatically satisfied and the Adler zeroes will appear only at one vertex in the remaining  $G_{\alpha i}(s)$ .

I believe this formalism should be much easier to apply, and physically more transparent, than e.g., the formalism of refs.[13, 14] where one multiplies the whole PWA's by real functions  $\alpha_i^p(s)$ . I have made some initial calculations along these lines, and seen that it is easy with appropriate choices of the  $C_{\beta p}(s)$  to obtain the  $f_0(980)$  either as a dip or as a peak in the cross section. But more quantitative applications are left for further work.

# 2.7 Comparison with the N/D method and the K-matrix. Physically acceptable analyticity.

For a single resonance and one threshold our function  $G^2(s)$  is the N function, while our  $P^{-1}(s)$  is the D function of the N/D method. For the more general case of many channels and many resonances there is no clear connection between the parameters in eq. (1) and those of a matrix form of N/D[28]. But, much of the same philosophy of N/D methods is also present in the UQM: Given a model for  $G_{\alpha i}(s)$  analyticity and unitarity constrain the form of the propagator  $P_{\alpha\beta}$ .

As to the relation between the K-matrix formalism and the UQM, one obtains the K-matrix corresponding to the matrix (1) by simply putting  $Im\Pi_{\alpha\beta}(s) = 0$ :

$$\hat{K}_{ij}(s) = (\rho_i \rho_j)^{1/2} K_{ij}(s) = \sum_{\alpha\beta} G^{\dagger}(s)_{i\alpha} [m_{0,\alpha}^2 + Re\Pi_{\alpha\beta}(s) - s]^{-1} G_{\beta j}(s) . \tag{32}$$

where  $\rho_i = k_i/\sqrt{s}$ .

The expression (1) is regained from the familiar formula:

$$A = \hat{K}(1 - i\hat{K})^{-1} . {33}$$

Note that the mass shift term  $Re\Pi_{\alpha\beta}(s)$  remains in our K-matrix. In particular, thresholds which have not yet opened contribute to  $Re\Pi_{\alpha\beta}(s)$ . Thus the UQM can be looked upon as a particular way of parametrizing the K-matrix in a way which is consistent with analyticity and dispersion relations, whereby one has a simple physical interpretation of the parameters.

By adding the  $Im\Pi_{\alpha\beta}(s)$  terms to the propagator one unitarizes the model and sums over the imaginary parts of an infinite series of loop diagrams (Fig. 1c). But to add the  $Re\Pi_{\alpha\beta}(s)$  terms is equally important. In many models such terms from nearby closed thresholds are omitted, wheras I find it essential to include a complete set of nearby flavour related thresholds. Through these one includes the mixing and mass shifts of the bare states with the continuum of meson pairs.

By omitting also the  $Re\Pi_{\alpha\beta}(s)$  terms from the denominator one obtains the bare matrix:

$$B_{ij}(s) = \sum_{\alpha} G^{\dagger}(s)_{i\alpha} [m_{0,\alpha}^2 - s]^{-1} G_{\alpha j}(s) .$$
 (34)

Since the bare masses and the functions  $G_{\alpha i}(s)$  determine the PWA  $A_{ij}$  through the scheme described above, there is a one to one correspondence between the bare and the physical masses, once the functions  $G_{\alpha i}(s)$  are given.

One can gain some physical intuition for the UQM formalism, by viewing the dispersion relation for  $Re\Pi(s)$  as the limiting case of the familiar second order perturbation formula for a mass shift  $\Delta E = \sum_i |<\alpha|H|i>|^2/(E-E_i)$ . Each piece of the continuum shifts the  $q\bar{q}$  state at the same time as the continuum is mixed into the state, with an amplitude  $<\alpha|H|i>/(E-E_i)$ . The sum of the squared mixing

amplitudes  $\sum_i |<\alpha|H|i>|^2/(E-E_i)^2$  again corresponds to the above  $-\frac{d}{ds}Re\Pi(s)$  =  $-\frac{1}{\pi}\int Im\Pi(s')/[s-s']^2ds'$ . But, in contrast to second order perturbation theory the dispersion relation formulas are "exact" in the sense that they solve the coupled channel model exactly.

It is important to emphasize that the function  $\Pi_{\alpha\beta}(s)$  must in general satisfy a dispersion relation like the one in eq.(5), whereby one automatically has physically correct analytic properties for an arbitrary form factor. But in the literature one often finds violations of this rule. A few examples should clarify this point:

If one would put  $\Pi(s) \propto k(s)/\sqrt{s}$ , i.e. make it proportional to the relativistic phase space factor, (which would be reasonable for Im  $\Pi(s)$  if one had pointlike hadrons) and use it both for the real and imaginary parts, one would have a spurious pole and cut at s=0 in the physical region. The correct procedure is to calculate the real part from a dispersion relation, whereby one gets the Chew-Mandelstam function, which is more complicated and has a logarithmic large s behaviour (one needs one subtraction constant because of the logarithmic divergence). Then one has no spurious pole nor cut at s=0.

An even simpler example is given by the function  $(4m^2 - s)^{1/2}/s$ , which also has a spurious pole. But, defining the function through the dispersion relation and its cut (now one needs no subtraction constant) one gets  $(4m^2 - s)^{1/2}/s - 2m/s$  i.e., one automatically subtracts the spurious pole at s = 0 from the physical sheet. [On the second sheet the pole remains, but does no harm: There the function is  $-(4m^2 - s)^{1/2}/s - 2m/s$ .] As a third example we take a finite cut as given by the function  $[(4m^2 - s)(s - \Lambda^2)]^{1/2}$ . The dispersion relation automatically subtracts a polynomial, which guarantees that the function vanishes asymptotically in the physical region: One gets  $[(4m^2 - s)(s - \Lambda^2)]^{1/2} - s + 2m^2 + \Lambda^2/2$ .

These added terms are not small nor insignificant. They alter the model predictions in a very crucial way, giving e.g., the sharp rise in  $Re\Pi(s)$  above the threshold (see Fig. 2). But as already mentioned, in the literature one often encounters models, which either disregard the real part entirely, or uses some variant of the physically unacceptable forms discussed above. Such forms might work within a limited energy region, if the spurious singularities are very far away, but would certainly fail if one considers several thresholds and a large energy region from threshold to 1.5 GeV, like in the present model.

#### 3. Comparison with data on the lightest scalar mesons.

#### 3.1 Parameters and form factor

As discussed in the previous section the PWA's of eq. (1) are defined once one has a model for the vertex functions  $G_{\alpha i}(s)$  in eq. (2) or (30) and the bare masses of eq. (3). For the latter it is natural to assume an "ideal" and isospin symmetric structure such that the bare  $u\bar{u}$  or  $d\bar{d}$  mass  $m_0$  is a free parameter, while the  $u\bar{s}$  and  $d\bar{s}$  bare masses are given by  $m_0 + m_s$  and the  $s\bar{s}$  bare mass by  $m_0 + 2m_s$ , where  $m_s$ 

is the bare strange constituent mass.

For the bare couplings  $\gamma_{\alpha i}$  we use the OZI rule giving connected flavour symmetric couplings of eq. (24). The actual numbers are given in Table 1 for general values of the pseudoscalar mixing angle  $\delta_P$ , which measure the deviation from the ideal states. The value of  $\delta_P$  is fixed to  $-54^{\circ}$  (which is equivalent to a mixing angle  $\theta_P = \delta_P + \cot^{-1}\sqrt{2} = -19^{\circ}$  for the angle measuring the deviation from pure  $SU3_f$  states). Such a value is close to what has been measured in other contexts. (E.g. linear mass matrix formulas give  $\delta_P = -58^{\circ}$ , quadratic  $-46^{\circ}$ , a recent crystal ball experiment[29] quotes  $-52.2^{\circ}$ , Akers et al.[30] has  $\delta_P = -53,7^{\circ}$ , while Gilman and Kaufman[31], Baghi et al.[32] and Donoghue et al. find [33]  $\delta_P \approx -55^{\circ}$ . The results are not too sensitive to its actual value as long as it is in this ball park. All the above determinations assume the mixing angle to be the same at the  $\eta$  as at the  $\eta'$  mass. This need not exactly be the case, since mixing angles are in general mass dependent; cf. our  $\delta_S(s)$  below. This same simplifying assumption for  $\delta_P$  is made also in this paper. With our sign conventions the  $\eta$  and  $\eta'$  states are given by:

$$|\eta\rangle = -\sin\delta_P|u\bar{u} + d\bar{d}\rangle/\sqrt{2} - \cos\delta_P|s\bar{s}\rangle, |\eta'\rangle = +\cos\delta_P|u\bar{u} + d\bar{d}\rangle/\sqrt{2} - \sin\delta_P|s\bar{s}\rangle.$$
(35)

$$a_{0} - \sqrt{2} \sin \delta_{P} \qquad K\bar{K} \qquad \pi \eta' \\ A_{0} - \sqrt{2} \sin \delta_{P} \qquad 1 \qquad \sqrt{2} \cos \delta_{P}$$

$$K\pi \qquad K\eta \qquad K\eta' \\ K_{0}^{*} \qquad \sqrt{\frac{3}{2}} \qquad -\sqrt{\frac{3}{2}} \cos(\delta_{I} - \delta_{P}) \sqrt{\frac{3}{2}} \sin(\delta_{I} - \delta_{P})$$

$$u\bar{u} + d\bar{d} \qquad \sqrt{3} \qquad 1 \qquad \sin^{2} \delta_{P} \qquad -\sin(2\delta_{P})/\sqrt{2} \cos^{2} \delta_{P} \\ s\bar{s} \qquad 0 \qquad \sqrt{2} \qquad \sqrt{2} \cos^{2} \delta_{P} \qquad \sin(2\delta_{P}) \sqrt{2} \sin^{2} \delta_{P}$$

Table 1. The relative Clebsch-Gordan coefficients for the coupling constants as given by the trace of eq. (24). The pseudoscalar mixing angle relative to the ideal frame is fixed at  $\delta_P = -54^{\circ}$ , while  $\delta_I = \cot^{-1} \sqrt{2} = 35.26^{\circ}$  is the ideal mixing angle.

More generally, one could allow for contributions from disconnected, OZI rule violating diagrams for the bare couplings, like  $\gamma'_{\alpha i} = \gamma' Tr[\mathcal{M}_{A_i}] Tr[\mathcal{M}_{B_i} \mathcal{M}_{C_{\alpha}}]$  or  $\gamma'_{\alpha i} = \gamma'' Tr[\mathcal{M}_{A_i}] Tr[\mathcal{M}_{B_i}] Tr[\mathcal{M}_{C_{\alpha}}]$ , which would introduce more parameters, and whereby the bare couplings involving the neutral members  $(\eta, \eta', f_0, f'_0)$  would be different.

Fig. 3. The  $K^*$  branching ratios into  $K\pi$  for the resonances on the  $K^*$  trajectory as a function of the squared resonance mass. The branching ratios fall as the square of the function in eq. (36) with  $k_0=0.63~{\rm GeV}^2$ . A similar exponentially falling behaviour is seen[6] for the branching ratios into  $\pi\pi$  for the resonances on the  $f_J$  and  $\rho_J$  trajectories. See text.

Note however, that our physical couplings do not obey the OZI rule, because of the nonzero value of the pseudoscalar mixing angle  $\delta_P$ , and because the loops included in our formalism generate a scalar meson mixing angle  $\delta_S(s)$ . It is possible that most of the OZI violation found is of this nature, coming from mixing in the mass matrix; therefore for simplicity, we assume as a starting point that the disconnected diagrams in the bare couplings can be put = 0. Of course, if e.g. a nearby gluonium state would be present, this assumption would have to be relaxed.

Since the data start only a few 100 MeV above the thresholds, they are not sensitive to the exact positions of the Adler zeroes  $s_{A_i}$  near s=0, provided these are small enough or of the order 0.1 GeV<sup>2</sup>. Thus we put all  $s_{A_i}=0$ , except in the case of the  $K\pi$  and the  $\pi\pi$  thresholds. For  $\pi\pi$  we put it equal to the current algebra value  $s_{A_{\pi\pi}}=m_{\pi}^2/2$  (although  $s_{A_{\pi\pi}}=0$  would work just as well). For  $K\pi$  we let the fit find the best value, which turns out rather large and negative  $s_{A_{K\pi}}=-0.42$  GeV<sup>2</sup>. Current algebra including corrections from chiral perturbation theory[34] would predict this to be closer to zero. By modifying the flavour symmetry prediction for the  $K\pi$  coupling, such that it is 10-15% larger than predicted by the Clebsch-Gordan coefficient of  $\sqrt{3}/2$  of table 1, one could fit the data with a smaller  $s_{A_{K\pi}}$ . Thus this determination of  $s_{A_{K\pi}}$  should not be taken too seriously.

Finally for the form factor  $F_i(s)$  one assumes the simple Gaussian form:

$$F_i(s) = \exp[-k_i^2(s)/(2k_0^2)] . (36)$$

This, no doubt, is the most drastic assumption of the model. It is used because it works, and because forms of this kind are obtained in the quark pair creation model (QPCM) [23]. There, it is given by the overlap of the three  $q\bar{q}$  wave functions of the three hadrons at the vertex times a matrix element for the  $^3P_0$  quark pair creation. With wave functions of Gaussian shape one gets a similar Gaussian factor, multiplied by a polynomial in s. The cutoff parameter  $k_0$  is then related to the hadron size R through  $k_0 = \sqrt{6}/R$ , from which with  $R \approx 0.7$  fm one would estimate  $k_0$  to be of the order 0.6-0.8 GeV/c. In the fit one finds  $k_0 = 0.56$  GeV/c. Including another cutoff parameter at the quark pair creation vertex the Orsay group[35] can account for a smaller cutoff parameter  $k_0$ .

There is another crude phenomenological argument for a form factor of this form: If one plots the elastic branching ratios for resonances on the leading trajectory (i.e the  $K\pi$  branching ratios for the  $K_J^*$ , see Fig. 3, or the  $\pi\pi$  branching ratio for the  $f_J$  or  $\rho_J$  trajectory[6]) one finds that they fall exponentially with squared mass or with  $k^2$  as the square of eq.(36) with  $k_0 \approx 0.63$  GeV/c. Of course this is not the same thing, but assuming that angular momentum barriers approximately cancel in the branching ratio, that the total widths grow much slower, perhaps linearly with s, and that each resonance has an exponential form factor similar to (36) in their partial widths to exclusive twobody channels etc., one can argue that there is some experimental support for such a shape and that the  $k_0$  parameter is about the same for all mesons.

No doubt,  $F_i(s)$  is in reality much more complicated than this. It should in principle include all the left hand cuts. But since the left hand singularities lie much farther away than the unitarity cuts, which we have included in detail, one can expect that the form (36) need not be too bad an approximation.

In table 2 below the parameters of the model are summarized:

| The over all dimensionless coupling constant      | $\gamma$       | 1.1395                 |
|---|----------------|------------------------|
| The $u\bar{u}$ and $d\bar{d}$ bare $0^{++}$ mass  | $m_0$          | $1.420~{ m GeV}$       |
| The constituent bare strange quark mass           | $m_s$          | $100~{\rm MeV}$        |
| The cutoff parameter                              |                | $0.56~\mathrm{GeV/c}$  |
| The Adler zero for $K\pi$                         | $s_{A_{K\pi}}$ | $-0.46 \; {\rm GeV^2}$ |
| The parameter enhancing the $\eta\eta'$ couplings | $\beta$        | 1.6                    |

Table 2. The parameters of the model. In addition, the pseudoscalar mixing angle  $\delta_P$  is fixed to a conventional value of  $-54^{\circ}$ , and the Adler zero for  $\pi\pi$  is given the current algebra value  $m_{\pi}^2/2$ , while for the remaining channels the Adler zeroes  $s_{A_i}$  are put = 0. Other constants used in the model include the pseudoscalar masses and the Clebsch-Gordan coefficients of Table 1.

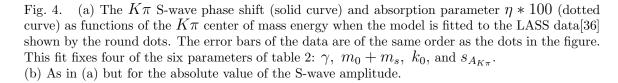


Fig. 5. The  $K\pi$  Argand diagram for the same fit as in Fig. 4. The numbers indicate the  $K\pi$  center of mass energy in MeV.

# **3.2.** The $K_0^*(1430)$ and the $K\pi$ S-wave.

It is natural to start the data comparison with the  $K\pi$  S-wave, since this is the simplest to understand, having only one resonance, the  $K_0^*(1430)$ , and in addition the experimental data are rather good. The comparison of the fit to the LASS data[36] is shown in Figs. 4a,b. The older data of Estabrooks et al.[37] are very similar but have larger error bars. The error bars of the LASS data are of the same magnitude as the dots in the figures. Fig. 4a shows the S-wave phase shift, while Fig. 4b shows the absolute magnitude of the amplitude (in Argand units). The corresponding Argand diagram is shown in Fig. 5. As can be seen the model has no difficulty in fitting the data rather well. These data essentially fix four of the parameters in Table 2:  $\gamma$ ,  $m_0+m_s$ ,  $k_0$  and  $s_{A_{K\pi}}$ . We say essentially, since some of the parameters are strongly correlated, in particular  $k_0$  and  $\gamma$ , and in practice because of the time consuming numerical integration in eq. (5) one must keep  $k_0$  fixed.

The parameters of the  $K_0^*(1430)$  also turn out to be rather close to the conventional ones (cf. Table 3). The BW mass is at 1349 MeV where the phase shift passes 90°, and the BW width is 398 MeV with negligible correction from eq. (15), since  $Re\Pi(s)$  is almost flat at 1350 MeV. The nearest pole is also where one normally expects it on the third sheet at  $[Re(s)]^{1/2} = 1440$  MeV, with an imaginary part -Im(s)/m = 320 MeV (Since the  $K\eta$  coupling almost vanishes this threshold is very weak and, in fact, there is an image pole on the second sheet at almost the same position).

Fig. 6. (a) The  $\pi\eta$  S-wave Argand diagram as predicted by the model when four of the parameters of table 2 are fixed by the  $K\pi$  data of Fig. 4 and  $m_s=100$  MeV. Note the sharply falling amplitude after the  $K\bar{K}$  threshold due to the strong absorption to this channel, which partly explains the narrow  $a_0(980)$  shape. The numbers are the center of mass energies in MeV.

(b) As in (a), but for the phase shift (solid curve) and absorption parameter (dotted curve) plotted as a function of  $\pi\eta$  center of mass energy.

Fig. 7. The  $a_0(980)$  resonance shape (solid curve) as predicted (not fitted) by the same model and parameters as in Figs. 4 and 6, and compared with the data of Armstrong et al.[38] from central production of  $\pi\pi\eta$  in 300 GeV pp collisions. The background (dashed curve) is a rough estimate of the reflection of other contributions to the experimental distribution and is added to the model prediction. Note that in spite of the inherently large width as measured by  $-Im\Pi(s)/m \approx 400$  MeV or by the imaginary part of the pole position the predicted peak width is rather narrow  $\approx 100$  MeV.

# 3.3. The $a_0(980)$ and the $\pi\eta$ S-wave.

When turning to the  $\pi\eta$  data for the  $a_0(980)$  there is only one new parameter,  $m_s$ , whose value one expects to be close to 100 MeV. And in fact, the fit allows for this value, therefore it is fixed at 100 MeV. The value 100 MeV is slightly lower than what is usually quoted in the light sector (e.g., the mass spittings of  $\phi - K^*$  or  $K^* - (\rho, \omega)$  is about 120 MeV.) But, part of this splitting is renormalized by the unitarity effects we include, and in the fits to the other light multiplets[21] values close to 100 MeV were found. A better comparison is with the  $D_s - D$  splitting of 99.1  $\pm$  0.6 MeV, since here unitarity effects are smaller.

The data for the  $a_0(980)$  is much poorer than for the  $K_0^*(1430)$ . In Fig. 6a the Argand diagram for the  $\pi\eta \to \pi\eta$  S-wave is shown, and Fig. 6b shows the phase shift with the absorption parameter. Fig. 7 shows the the prediction for the  $a_0(980)$  peak compared with the data of Armstrong et al.[38] of centrally produced  $\eta\pi\pi$  in pp collisions. It is significant that the model predicts a rather narrow peak at the right mass. This low mass comes out right since the mass shift is the largest at the threshold, and the three thesholds for the  $a_0$ :  $\pi\eta$ ,  $K\bar{K}$ ,  $\pi\eta'$  (Fig. 2b) lie close to each others, while the corresponding ones for  $K_0^*$ :  $K\pi$ ,  $K\eta$ ,  $K\eta'$ , (Fig. 2a) are much more spread out in energy and the middle one,  $K\eta$ , almost decouples. Again the rather narrow peak structure of about 100 MeV seems at first very surprising, considering the very large imaginary part (cf. in Fig. 2b,  $Im\Pi(s)/m \approx 400$  MeV). This is due to several contributing effects, which we list in their order of importance:

- i) The large negative slope of  $Re\Pi(s)$  below the  $K\bar{K}$  threshold, which according to eq.(6) renormalizes the BW width by a large factor, which is close to 5 at  $\sqrt{s} = .98$  GeV:
- ii) The strong absorption above the  $K\bar{K}$  threshold (cf. the Argand diagram of Fig. 6a) making the amplitude drop fast in magnitude above this threshold;
  - iii) The Adler zero at s=0 reduces the amplitude somewhat near the threshold.

See also the discussion of pole position, Sec. 3.5, for another way of understanding the narrow peak.

## **3.4.** The $f_0(980)$ and $f_0(1300)$ and the $\pi\pi$ S-wave.

Finally we turn to the much more complicated  $\pi\pi$  S-wave shown in Fig. 8 together with the CERN-Munich[39], Cason et al.[40], Grayer et al.[41] and some lower energy experiments[42]. Here we have two resonances with complex energy dependent mixing. Now essentially all of our parameters except one are already fixed by the  $K\pi$  and  $\pi\eta$  data. But even without new parameters, the prediction for the phase shift is not too bad below 1.1 GeV. The additional parameter  $\beta$  is needed in order to fit the phase shift above this energy, which otherwise comes out about 40° too low. We chose this to be a factor in front of the  $\eta\eta'$  couplings, which thus violate the flavour symmetry

Fig. 8. (a) The Argand diagram of the  $\pi\pi$  S-wave as predicted (not fitted) by the model when 4 of the 6 parameters of table 2 are fixed by the  $K\pi$  data of Fig. 4 and  $m_s=100$  MeV (as in Figs.6-7) and  $\beta=1.6$ . The numbers are the center of mass energies in MeV.

(b) The same prediction as in (a) for the  $\pi\pi$  phase shift (solid curve) and absorption parameter  $\eta*100$  (dashed) as function of the center of mass energy, and compared with the CERN-Munich[39], Cason et al[40], Grayer et al.[41] and some low energy experiments[42].

predictions of Table 1, being increased by 60%. This determines our final parameter  $\beta=1.6$ . Of course this does not necessarily mean that this is the right choice. Equally well one could think of other effects, left out of the model, which could be faked by  $\beta$ . These include higher thresholds which enter at about the same energy as  $\eta\eta'$  in the 1.5 GeV region such as vector-vector or pseudoscalar-axial thresholds etc., or an effect due to the higher mass scalar resonances seen in this region.

In Figs. 9 and 10 the running masses are shown before, respectively after diagonalization of the mass matrix. Note that in the region of the two resonances the real parts of the two diagonal running masses are nearly degenerate (Fig. 9a) due to the mass shifts from the  $K\bar{K}$  threshold. Therefore the mixing angle (Fig. 10c) between the two resonances changes rapidly at the  $K\bar{K}$  threshold from being nearly ideal  $\delta_S \approx 0^\circ$  below 900MeV to  $\delta_S \approx -35.26^\circ$  where the states are close to being  $SU3_f$  eigenstates. Note that the large value of  $-Im(m_1^2)$  results in a very large BW width (880 MeV) of the first BW resonance ("the  $\sigma$ "). Fig. 10a,b shows the eigenvalues, with the BW masses given by the crossing points of the real parts with s. In Fig. 10 the  $f_0(980)$  does not appear as a BW resonance, but it is hidden under the complex and rapid energy dependent mixing. It is another linear combination of the two states, which appears when one analytically continues to the nearby poles.

## 3.5. Pole positions and BW resonance masses and widths.

When one asks the question, where are the poles of the resonances in this model with large imaginary parts, one is tempted to say: Who cares where the poles end up in the complex multisheeted structure of the s-plane! Each resonance may require many poles on different sheets for a full description of its pole structure. On the other hand one has a very simple bare spectrum, and a rather simple description of the data. The bare masses are strongly shifted nonperturbatively to some s values and sheet numbers, whose positions depend sensitively on the precise positions of where the thresholds are. Do we really learn anything fundamental from knowing the precise pole positions, apart from having numbers to put into the PDG tables? I am inclined to answer: not very much, they are of secondary importance! Of course, the experimental data, resonance shapes and threshold positions are very important in order to find the correct solution with a reasonable bare spectrum together with the other model parameters. But the actual positions of the poles depend more on the positions of the thresholds and on Clebsch Gordan coefficients, than on the model parameters.

The actual pole positions do tell us something of the analytic structure of the solution found, and can throw some light on resonance shapes. E.g., the fact that the nearest  $a_0(980)$  and  $f_0(980)$  poles are found on the second sheet, although their Re  $(s_{pole})$  are above the  $K\bar{K}$  threshold, throws some light on why these are narrow. Normally with two open thresholds the nearest resonance pole is expected on the third sheet. The fact that it often turns up on the second sheet explains partly their shapes: The nearest place to the pole in the physical region is at the threshold, since

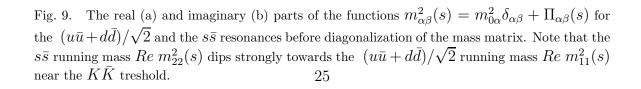


Fig. 10. The real (a) and imaginary (b) parts of the eigenvalues of the mass matrix  $m_{\alpha'}^2(s)$  after diagonalization, and (c) the scalar mixing angle  $\delta_S(s)$ . The crossing points with s (dashed) in (a) give the BW masses. Note that  $\delta_S(s)$  is almost real at the energies of the BW masses, and has a large imaginary part in the  $K\bar{K}$  threshold region. For low energies the mixing is nearly ideal  $(\delta_S=0^\circ)$ , wheras above 1.1 GeV one has nearly pure  $SU3_f$  eigenstates  $(\delta_S=-35.26^\circ)$ . At the lighter BW mass  $\sqrt{s}=0.86$  GeV one has an extremely broad (880 MeV) near  $(u\bar{u}+d\bar{d})/\sqrt{2}$  BW resonance (the " $\sigma$ ") while at 1186 MeV one has a near  $SU3_f$  octet BW resonance. On the other hand, when one analytically continues to the nearest pole, these combine linearly to give one very "narrow" almost pure  $s\bar{s}$  state [the  $f_0(980)$ ], which lies on the second (not third) sheet. See text for discussion.

one must go around the  $K\bar{K}$  cut to see the pole. Therefore, a narrow peak appears at the threshold in spite of a very large imaginary part of the pole position, and in spite of the fact that  $Re(s_{pole})$  is about 90 MeV above the  $K\bar{K}$  threshold. Of course, as explained above one can also understand the narrow  $a_0(980)$  by the arguments given earlier by the structure of the amplitudes in the physical region at  $Re(s) + i\epsilon$ .

In Table 3 I list the Breit-Wigner masses, widths (in MeV) and mixing angles together with the nearest pole positions, the Riemann sheet of the poles and mixing angles at the poles. Note that the  $a_0$  and  $f_0$  lie on the second sheet although the  $K\bar{K}$  threshold is open at the pole mass, as was already discussed above. Similarly the second  $f_0$  lies on the 3rd sheet although the  $\eta\eta$  threshold is open, and one normally would expect it at the 5th sheet. The  $a_0$  width in the  $\Gamma_{BW}$  column is the peak width since it is not possible to define a BW width.

The mixing angle  $\delta_S$  is such that at the BW mass of the first  $f_0$ , whose BW width is enormous, 880 MeV,  $\delta_S$  is small, i.e. one has an almost pure  $(u\bar{u}+d\bar{d})/\sqrt{2}$  state with a little mixture of  $s\bar{s}$ . The sign of this mixing such that it is mainly an  $SU3_f$  singlet state. This BW resonance we interpret as the " $\sigma$ ". On the other hand, when one analytically continues to the pole with lowest mass one has another linear combination of the two resonances: A narrow almost pure  $s\bar{s}$  state (but with a large  $i\text{Im}\delta_{S,pole}=i39^\circ$ ). This is our  $f_0(980)$ . See also our discussion in Sec 2.3 of how two broad resonances can make one narrow. The heavier  $f_0(1300)$  is close to an SU3<sub>f</sub> octet both at the BW mass and at the pole position. Also the mass of the heavier state is similar both at the pole (1202 MeV) and when measured as a BW resonance (1186 MeV).

| Resonance     | $m_{BW}$ | $\Gamma_{BW}$            | $\delta_{S,BW}$             | $(Re\ s_{pole})^{\frac{1}{2}}$ | $\frac{-Ims_{pole}}{m_{pole}}$ | Sheet nr | $\delta_{S,pole}$         |
|---------------|----------|--------------------------|-----------------------------|--------------------------------|--------------------------------|----------|---------------------------|
| $a_0$         | 987      | $\approx 100^{\dagger)}$ |                             | 1084                           | 270                            | II       |                           |
| $K_0^*$       | 1349     | 398                      |                             | 1441                           | 320                            | III      |                           |
| Lighter $f_0$ | 860      | 880                      | $-9^{\circ} + i8.5^{\circ}$ | 1006                           | 33.7                           | II       | $0.4^\circ + i39^\circ$   |
| Heavier $f_0$ | 1186     | 350                      | $-32^{\circ}+i1^{\circ}$    | 1202                           | 338                            | III      | $-36^{\circ} + 2^{\circ}$ |

Table 3. Breit-Wigner masses, widths (in MeV) and mixing angles together with the nearest pole position parameters, Riemann sheet number and mixing angles at the poles. Except for the  $\delta_{S,BW}$  at the light  $f_0$  the three other mixing angles are given with respect to the  $s\bar{s}$  state. The heavy  $f_0$  is thus close to an  $SU3_f$  octet, for which  $\delta_S = -35.26^\circ$ , while the lighter BW  $f_0$  is a near  $(u\bar{u} + d\bar{d})/\sqrt{2}$  state (the  $\sigma$ ). But at the poles one has other linear combinations of the two resonances such that the lighter is a narrow almost pure  $s\bar{s}$  state, the  $f_0(980)$ .

<sup>†)</sup> The  $a_0$  width in the  $\Gamma_{BW}$  column is the peak width as it is here not possible to define a BW width. See text.

Our solution suggests a novel way to resolve the old question: Where is the  $\sigma$  meson? From the low energy side the  $\pi\pi$  interaction looks very much as if there

would only be an extremely broad (880 MeV) BW resonance with a mass of 860 MeV, and with a composition near  $(u\bar{u}+d\bar{d})/\sqrt{2}$ . The fact that the running mass is not constant makes the effective  $\sigma$  mass slightly vary depending on what energy one is sensitive to. It is interesting that this prediction of the  $\sigma \to \pi\pi$  width is close to the values predicted in the linear  $\sigma$  model and in extensions of the Nambu–Jona-Lasinio model[43].

On the other hand as one approaches the  $K\bar{K}$  the shold the two resonances experience a dramatic s-dependent mixing, such that at the  $K\bar{K}$  threshold the relevant linear combination appears as an almost pure  $s\bar{s}$  pole [the  $f_0(980)$ ]. We find the pole to be a little above the threshold and on the second sheet, with its precise position rather sensitive to model parameters. But, it is always a few MeV from the  $K\bar{K}$  threshold.

# 4. Concluding remarks.

In 1972 Feynman[2] wrote in connection with the problem of how to treat virtual hadronic loops, needed by self consistency in the quark model, that "it is the most important problem in the theory of strong interactions", but continued that "no calculation of such virtual strong interactions in any problem has ever been successful". He thought this "dead end is a result of lack of imagination of how to get further".

No doubt, these were strong words, and certainly we have made a lot of progress to understand virtual hadronic states since 1972, but the progress has been rather slow, possibly because too many theorists really thought that one had reached a "dead end", and looked for other approaches guided by QCD. Thereby the nonperturbative methods and related problems of the sixties were "swept under the rug".

Today it seems more and more obvious that attempts where one, starting directly from the QCD Lagrangian, tries to solve the nonperturbative light hadron spectrum, has come to another "dead end", in spite of the heroic attempts of e.g., lattice QCD. This seems all the more obvious, with the present solution of the scalar nonet at hand, which I believe to be close to the true solution, although certainly improvements can and should be done. To disentangle all the complicated threshold singularities, shifting the poles to some strange corners of the the many-sheeted structure of the complex s plane, and then try to understand why some peaks like the  $a_0(980)$  or  $f_0(980)$  are narrow in spite of their large couplings, seems to be an impossible task to resolve directly from the QCD Lagrangean. It would require inclusion of fermionic loops and too much computing power, if one would not know how to proceed through some intermediate steps.

Such an intermediate step which I believe should be useful, is to use QCD to calculate, or at least understand qualitatively, the parameters used in the UQM, i.e., the overall coupling constant  $\gamma$ , the cutoff parameter  $k_0$  and the bare masses, when the mass shifts and couplings to the lightest thresholds have been unfolded.

A few comments are in order as to the meaning of the bare masses found in this paper. The value of  $m_0$  depends on the cutoff parameter  $k_0$  and on the number of

thresholds, which have been included. The larger the cutoff and the more thresholds included in the UQM, the larger will  $m_0$  be. Furthermore, if one also includes tadpole graphs with hadron loops, these have no imaginary part, but would contribute to  $Re\Pi$ , and shift  $m_0$  down, partly cancelling the mass shift from the thresholds. Thus the bare mass  $m_0$  is model dependent. On the other hand, the bare constituent strange quark mass  $m_s$  is less dependent on distant singularities, since in the mass difference  $m_0(s\bar{s})-m_0(u\bar{u})=2m_s$  the above effects essentially cancel. Similarly OZI rule violating mixing between resonances  $(\delta_S)$  is less dependent on distant thresholds, since when one sums over complete sets of F-coupled and D-coupled flavour related thresholds their contribution to off diagonal elements in the mass matrix is small[21, 45]. Only the overall bare mass scale  $m_0$  can depend strongly on distant singularities.

The model we have found for the scalar nonet is, in principle, not very different than what one would assume for any of the other  $q\bar{q}$  nonets with finite decay widths. For these one must always have an input mass scale  $m_0$  and a strange quark mass  $m_s$  and an overall coupling parameter which, together with flavour symmetry describe the finite widths. Also the cutoff parameter must, in principle, exist by self consistency, although one implicitly assumes that things do not depend on it. Our solution has the same four parameters plus only two additional phenomenological parameters, ( $\beta$  and  $s_{A_{K\pi}}$ ), which may be just artifacts of the things left out of the model. Apart from the  $\beta$  parameter flavour symmetry is broken in our scheme most importantly by the pseudoscalar mass differences and by the small  $m_s$ .

An important feature of the model is that the  $a_0(980)$  and the  $f_0(980)$  have very large components of  $K\bar{K}$  (and also some  $\eta'\pi$  or  $\eta\eta$  etc.) in their wave functions. We estimate the  $K\bar{K}$  component to be dominant in the  $a_0(980)$  near the peak being about 4-5 times larger than the  $q\bar{q}$  component. This does of course not mean that the  $a_0(980)$  or the  $f_0(980)$  are  $K\bar{K}$  bound states; they owe their existence to the  $q\bar{q}$  component. But, it is important to note that this will make these states look "as if they were  $K\bar{K}$  states". E.g., their widths to  $\gamma\gamma$  will be reduced by this same factor of 4-5, and thus a reduced  $\gamma\gamma$  width does not prove that they are  $K\bar{K}$  molecules, as has beed argued by Close and Barnes and collaborators[44]. One should not compare the  $K\bar{K}$  molecule model with a too naive  $q\bar{q}$  model, without the large virtual  $K\bar{K}$  component in the wave function.

Finally a natural question many readers certainly ask: Why is it that the scalar mesons are so much more sensitive to nonperturbative unitarity and analyticity effects compared to the other light nonets? And a related question: Why has not the solution presented here not been found previously?

To answer the first question one observes two special features for the scalars:

(i) The over all squared coupling coupling constant  $\gamma^2$  is about 5-6 times larger for the scalars than for the vector nonet. This can be seen already by comparing the  $K_0^*(1430)$  width[7] of 287 MeV, which is 5.7 times larger than the  $K^*$  width of 50 MeV. A better comparison taking into account phase space etc. is found by determining a corresponding dimensionless  $\gamma^2$  parameter for the vectors from the width expression:  $(m\Gamma)_{K^*} = 3/2\gamma^2(4k^2)k/\sqrt{s}$ , which also gives a factor of about 5

- smaller  $\gamma^2$ . Theoretically this is roughly what one also expects from spin counting or  $SU6_W$  symmetry, which would predict a factor of 3. Thus the pseudoscalar thresholds are about five times stronger for the scalar mesons than for the vector mesons and consequently unitarity effects are much more important.
- (ii) The second feature which makes the thresholds more important for the scalars is that these are S-wave thresholds. Therefore one has strong square root cusps in  $\Pi(s)$  with a discontinuous first derivative. For P-wave and higher angular momenta this is smoothened out by the angular momentum factor  $k^{2\ell}$ . Thereby the scalars are much more sensitive to the threshold positions, especially when the resonance turns up near a threshold as is the case for the  $a_0(980)$  and for the  $f_0(980)$ .

As to the second question, why this solution has not been found previously, one notes that (disregarding our first short note[19]), no one has tried to fit simultaneously the whole nonet taking into account all the light pseudoscalar thresholds, putting in physically acceptable analyticity properties etc.

Acknowledgements. Useful discussions with the Orsay group, in particular with A. Le Yaouanc, L. Olivier, O. Pène and J.C. Raynal, and with the meson team of the Particle Data Group[7], especially Matts Roos, are greatfully acknowledged. M. Sainio helped me to find references on Adler zeroes and scattering lengths. I also thank J. Soffer for an invitation to Centre Physique Theorique, in Marseille, where part of this work was written up.

# 1. \*

#### References

- [1] N. Isgur, Proc Int. Conf on High Energy Physics, Dallas USA, Ed. J.R. Sanford AIP Conf. Proc. 272 Vol 1 (1992) p. 33;
  - D. V. Bugg, Proc. Int. Europhysics Conf. on High Energy Physics, Marseille, France, Eds. J Carr, M Perrottet, Editions Frontiers (1994) p. 717;
  - C. Amsler, Int. Conf on High Energy Physics, Glasgow 20-27 July 1994. Plenary talk, Zürich preprint UZH-PH-50/94.
- [2] R.P. Feynman, *Photon Hadron Interactions*, W.A. Benjamin Inc., Reading Mass. USA, (1972), pages 58 and 95;
  - A. Katz and H.J. Lipkin, Phys. Lett. **7** (1963) 44; H.J. Lipkin Phys. Lett. **72B** (1977) 249;
  - G. F. Chew, The Analytic S-Matrix, W.A. Benjamin Inc., New. York, 1966;
  - G. F. Chew and C. Rosenzweig, Phys. Rep. 41 (1978) 264;
  - G. Fogli and G.Preparata, Nuovo Cimento 48A (1978) 235;
  - A.C.A. Maciel and J. Paton, Nucl. Phys **B181** (1981) 277;
  - A.W. Thomas et al., Phys. Rev. **D24** ((1981) 2161;
  - E. Van Beveren et al., Phys. Rev. **D21** (1980) 773; **D27** (1973) 1527; Z. Phys. **C19** (1983) 275.

- [3] J. Weinstein and N. Isgur, Phys. Rev. Lett. **D48** (1982) 659; Phys. Rev **D 27** (1983) 588.
- [4] CBAR collaboration, C. Amsler et al., Phys. Lett.B 333 (1994) 277.
- [5] M. Boutemeur, Hadron 89 conf. proc. (Ajaccio, Corsica) p. 119.
- [6] N.A. Törnqvist, Nucl. Phys. B (Proc. Suppl.) 21 (1991) 196.
- [7] Particle Data Group, L. Montanet et al., Phys. Rev. **D50** (1994) 1173.
- [8] WA91 Collaboration, S. Abatzis et al., Phys. Lett. **B324** (1994) 509.
- [9] N.A. Törnqvist, Phys. Rev. Lett. 67 (1991) 556, and Z. Physik C61 (1994) 525;
  T.E.O. Ericson and Gabriel Karl, Phys. Lett. B 309 (1993) 426;
  M. Shmatikov, Bochum preprint 1995, RUB-MEP-7/95.
- [10] Y. Nambu and G. Jona-Lasinio, Phys. Rev. **122** (1961) 345.
- [11] A. Manohar and H. Georgi, Nucl. Phys. **B234** (1984) 189.
- [12] U-G. Meissner, Comm. Nucl. Part. Phys. 20 No 3 (1991) 119.
- [13] D.V. Bugg, V.V. Anisovich, A. Sarantsev and B.S. Zou, Phys. Rev. **D50** (1994) 4412; VV.Anisovich, D.V. Bugg, A,V. Sarantsev and B.S. Zou, Phys. Rev. **D50** (1994) 1972; B.S. Zou and D.V. Bugg, Phys. Rev. **D48** (1993) R3948; **D50** (1994) 591.
- [14] K.L. Au, D. Morgan and M.R. Pennington, Phys. Rev **D35** (1987) 1633;
   D. Morgan, and M.R. Pennington, Phys. Rev. **D48** (1993) 1185; **D48** (1993) 5422.
- [15] G. Janssen, B.C. Pearce, K. Holinde and J.Speth, "On the structure of the scalar mesons  $f_0(980)$  and  $a_0(980)$ ", Jülich preprint 1994.
- [16] N.N. Achasov, G.N. Shestakov, Phys. Rev. D 49 (1994) 5779.
- [17] R. Kaminski, L. Lesniak and J.-P. Maillet, Phys. Rev. **D50** (1994) 3145.
- [18] B.R. Martin, D. Morgan and G. Shaw, Pion-Pion Interactions in Parrticle Physics, (Academic Press, New York 1974);
  J.L. Basdevant and B.W. Lee, Phys. Lett., 29B (1969) 437; D2 (1970) 1680;
  O. Babelon et al., Nucl. Phys. B113 (1976) 445;
  R.H. Dalitz and S. Tuan, Ann. Phys. (N.Y.) 10 (1960) 307; R.H. Dalitz in Resonances Models and Phenomena, Proc. of the workshop, Bielefeld, Germany 1984, eds. S.Albeverio et al., Lecture Notes in Physics Vol. 21 (Springer, New York, 1984 pp. 1-26.
  - S. Flatté, Phys. Lett. **63B** (1976) 224;

- T.N. Truong, Phys. Rev. Lett. **67** (1991) 2260; Acta Phys. Pol. **B15** (1964) 633; L. Beldjoudi and T.N. Truong, Ecole Polytechnique preprint 1994, CPTH-A294-0294;
- J.L. Petersen, CERN yellow report (Febr. 1977) CERN 77-04.
- [19] N. A. Törnqvist, Phys. Rev. Lett 49 (1982) 624.
- [20] V. Weisskopf and E. Wigner, Z. Physik **63** (1930) 54.
- [21] For a review see: N.A. Törnqvist, Acta. Phys. Pol. B16 (1985) 503; Ann. Phys. (NY) 123 (1979) 1;
  - For vector and pseudoscalar mesons: M. Roos and N. A. Törnqvist, Z. Physik C5 (1980) 205;
  - For axial meson multiplets: N. A. Törnqvist, Nucl. Phys.  $\bf B203$  (1982) 268; For the tensor multiplet: Phys Rev  $\bf D29$  (1984) 121;
  - For baryons: N.A. Törnqvist and P. Żenczykowski, Phys.Rev. **D29** (1984) 2139; Z. Physik **C30** (1986) 83; Z. Physik C31 (1986) 439; P. Żenczykowski, Ann. Phys. (NY) **169** (1986) 453;
  - B. Silvestre-Brac and C. Gignoux, Phys. Rev. **D43** (1991) 3699.
- [22] For  $c\bar{c}$  and  $b\bar{b}$  mesons: N. A. Törnqvist, Phys.Rev. Lett.**53** (1984) 878; S. Ono et al., Phys. Rev. Lett. **55** (1985) 2938; Phys. Rev. **D34** (1986) 186; K. Heikkilä et al., Phys. Rev. **D29** (1984) 110; S. Ono et al., Z.Physik **C23** (1984) 59. H.-Y. Zhou and Y.-P. Kuang, Phys. Rev. **D44**) (1991 756.
- [23] A. Le Yaouanc, L. Olivier, O. Pène, J.C. Raynal, Phys. Rev. D8 (1973) 2223;
  D11 (1975) 1272;
  M. Chaichian and R. Kögerler, Ann. Phys. (N.Y) 124 (1980) 61.
- [24] L. Castillejo, F.J. Dyson, R.H. Dalitz, Phys. Rev. **D101** (1956) 45.
- [25] Y. Dothan and D. Horn, Phys. Rev. D1 (1970) 916;
  C. Rebbi and R. Slansky, Phys. Rev. 185 (1969) 1838.
- [26] N.A. Törnqvist, Helsinki preprint SEFT-R-1994-03. Phys. Rev. D in press.
- [27] S.L. Adler, Phys. Rev. **137B** (1965) 1022; **139B** (1965) 1638.
- [28] J.D. Björken, Phys. Rev. Lett. 4 (1960) 473.
- [29] C. Amsler et al., Phys. Lett. **B294** (1992) 451.
- [30] E. Aker et al., Nucl. Instrum. Methods **A321** (1992) 69.
- [31] F. Gilman and R. Kauffman, Phys. Rev. **D36** (1987) 2761.
- [32] B. Baghi et al., Phys. ReV.**D41** (1990) 2871.

- [33] J.F. Donoghue et al., Phys. Rev. Lett. **55** (1985) 2766.
- [34] V. Bernard, N. Kaiser, U-G. Meissner, Phys. Rev. **D43** (1991) R2757; **D44** (1991) 3698; Nucl. Phys. **357** (1991)129; **B364** (1991) 283.
- [35] Private communication with A. Le Yaouanc.
- [36] D. Aston et al., Nucl. Phys. **B 296** (1988) 493.
- [37] P. Estabrooks et al., Nucl. Phys. **B133** (1978) 490.
- [38] T.A. Armstrong et al., Z. Physik. C52 (1991) 389.
- [39] W. Ochs, Ph.D. thesis, Munich university, 1973 (unpublished); B. Hyams et al., Nucl. Phys. B64 (1973) 134.
- [40] N.M. Cason et al., Phys.Rev. **D** 28 (1983) 1586.
- [41] G. Grayer et al., Nucl. Phys. **B75** (1974) 189.
- [42] L. Rosselet et al., Phs. Rev. D15 (1977) 574:
  A. Zylberstejn, Ph.D. thesis, University of Paris, Orsay, 1972, (unpublished);
  E. W. Beier et al., Phys.Rev.Lett. 29 (1972) 511; 30 (1973) 399.
- [43] See e.g., T. Hatsuda and T. Kunihiro, Tsukuba preprint (1994) UTHEP-270 (to appear in Physics Reports);
   S. Weinberg, Phys. Rev. Lett. 65 (1990) 1177.
- [44] F.E. Close, Proc. Int. Conf. High Energy Physics, Dallas, Ed. J.R. Sanford, AIP Conf. Proc. No. 272 (1993) p. 562;
  F.E. Close and Z. Li, Z.Physik C54 (1992) 147; T. Barnes et al., Phys. ReV.D46 (1991) 2161; F.E. Close et al., Nucl. Phys. B389 (1993) 513.
- [45] P. Geiger and N. Isgur, Phys. Rev. **D** 47 (1993) 5050.

# Figure captions

- Fig. 1 The Born term for (a) the bare  $q\bar{q}$  resonances, for (b) the contact terms, and (c) the loops summed by the functions  $\Pi_{\alpha\beta}(s)$  in the inverse propagator.
- Fig. 2. (a) The real and the imaginary parts of the function  $m^2(s) = m_{0i}^2 + \Pi(s)$  for the  $K_0^*(1430)$  resonance plotted as a function of  $\sqrt{s}$ . Note the strong cusp at the  $K\eta'$  threshold and that the  $K\eta$  threshold essentially decouples because of the small coupling constant. The dashed curve is s, which crosses the running mass  $\text{Re}[m^2(s)]$  at the BW mass.
- (b) As in (a) but for the  $a_0(980)$  resonance. Note that the three thresholds have similar coupling strengths and that they lie much closer together than in (a). Therefore the large mass shift for  $a_0(980)$ . The dashed curve is s, which crosses  $\text{Re}[m^2(s)]$  at the BW mass.
- Fig. 3. The  $K^*$  branching ratios into  $K\pi$  for the resonances on the  $K^*$  trajectory as a function of the squared resonance mass. The branching ratios fall as the square of the function in eq. (36) with  $k_0 = 0.63$  GeV<sup>2</sup>. A similar exponentially falling behaviour is seen[6] for the branching ratios into  $\pi\pi$  for the resonances on the  $f_J$  and  $\rho_J$  trajectories. See text.
- Fig. 4. (a) The  $K\pi$  S-wave phase shift (solid curve) and absorption parameter  $\eta*100$  (dotted curve) as functions of the  $K\pi$  center of mass energy when the model is fitted to the LASS data[36] shown by the round dots. The error bars of the data are of the same order as the dots in the figure. This fit fixes four of the six parameters of table 2:  $\gamma$ ,  $m_0 + m_s$ ,  $k_0$ , and  $s_{A_{K\pi}}$ .
- (b) As in (a) but for the absolute value of the S-wave amplitude.
- Fig. 5. The  $K\pi$  Argand diagram for the same fit as in Fig. 4. The numbers indicate the  $K\pi$  center of mass energy in MeV.
- Fig. 6. (a) The  $\pi\eta$  S-wave Argand diagram as predicted by the model when four of the parameters of table 2 are fixed by the  $K\pi$  data of Fig. 4 and  $m_s = 100$  MeV. Note the sharply falling amplitude after the  $K\bar{K}$  threshold due to the strong absorption to this channel, which partly explains the narrow  $a_0(980)$  shape. The numbers are the center of mass energies in MeV.
- (b) As in (a), but for the phase shift (solid curve) and absorption parameter (dotted curve) plotted as a function of  $\pi\eta$  center of mass energy.
- Fig. 7. The  $a_0(980)$  resonance shape (solid curve) as predicted (not fitted) by the same model and parameters as in Figs. 4 and 6, and compared with the data of Armstrong et al.[38] from central production of  $\pi\pi\eta$  in 300 GeV pp collisions. The background (dashed curve) is a rough estimate of the reflection of other contributions to the experimental distribution and is added to the model prediction. Note that in spite of the inherently large width as measured by  $-Im\Pi(s)/m \approx 400$  MeV or by the

imaginary part of the pole position the predicted peak width is rather narrow  $\approx 100$  MeV.

- Fig. 8. The Argand diagram of the  $\pi\pi$  S-wave as predicted (not fitted) by the model when 4 of the 6 parameters of table 2 are fixed by the  $K\pi$  data of Fig. 4 and  $m_s = 100$  MeV (as in Figs.6-7) and  $\beta = 1.6$ . The numbers are the center of mass energies in MeV.
- (b) The same prediction as in (a) for the  $\pi\pi$  phase shift (solid curve) and absorption parameter  $\eta * 100$  (dashed) as function of the center of mass energy, and compared with the CERN-Munich[39], Cason et al[40], Grayer et al.[41] and some low energy experiments[42].
- Fig. 9. The real (a) and imaginary (b) parts of the functions  $m_{\alpha\beta}^2(s) = m_{0\alpha}^2 \delta_{\alpha\beta} + \Pi_{\alpha\beta}(s)$  for the  $(u\bar{u} + d\bar{d})/\sqrt{2}$  and the  $s\bar{s}$  resonances before diagonalization of the mass matrix. Note that the  $s\bar{s}$  running mass  $Re~m_{22}^2(s)$  dips strongly towards the  $(u\bar{u} + d\bar{d})/\sqrt{2}$  running mass  $Re~m_{11}^2(s)$  near the  $K\bar{K}$  treshold.
- Fig. 10. The real (a) and imaginary (b) parts of the eigenvalues of the mass matrix  $m_{\alpha'}^2(s)$  after diagonalization, and (c) the scalar mixing angle  $\delta_S(s)$ . The crossing points with s (dashed) in (a) give the BW masses. Note that  $\delta_S(s)$  is almost real at the energies of the BW masses, and has a large imaginary part in the  $K\bar{K}$  threshold region. For low energies the mixing is nearly ideal ( $\delta_S=0^\circ$ ), wheras above 1.1 GeV one has nearly pure  $SU3_f$  eigenstates ( $\delta_S=-35.26^\circ$ ). At the lighter BW mass  $\sqrt{s}=0.86$  GeV one has an extremely broad (880 MeV) near  $(u\bar{u}+d\bar{d})/\sqrt{2}$  BW resonance (the " $\sigma$ ") while at 1186 MeV one has a near  $SU3_f$  octet BW resonance. On the other hand, when one analytically continues to the nearest pole, these combine linearily to give one very "narrow" almost pure  $s\bar{s}$  state [the  $f_0(980)$ ], which lies on the second (not third) sheet. See text for discussion.

This figure "fig1-1.png" is available in "png" format from:

This figure "fig2-1.png" is available in "png" format from:

This figure "fig1-2.png" is available in "png" format from:

This figure "fig2-2.png" is available in "png" format from:

This figure "fig1-3.png" is available in "png" format from:

This figure "fig2-3.png" is available in "png" format from: